December 1973 LRP 77/73

A PLASMA BOX USING MAGNETIC MULTIPOLE CONFINEMENT

P.J. Hirt and M.Q. Tran

Centre de Recherches en Physique des Plasmas

ECOLE POLYTECHNIQUE FEDERALE DE LAUSANNE

December 1973

LRP 77/73

A PLASMA BOX USING MAGNETIC MULTIPOLE CONFINEMENT

P.J. Hirt and M.Q. Tran

A b s t r a c t

A plasma box using alternating magnetic multipole confinement is described. With disk shaped magnets a good confinement is achieved, the plasma lifetime being of the order of 200 μs. Consequently, a very low electron emission current (200 mA, heating power 250 VA) is required to maintain densities up to 2×10^{9} cm^{-3} in Argon, with an electron temperature of 2,5 eV and an ion temperature of 0,8 eV. The temperature ratio may be changed with a Maxwell demon between 2.0 and 5.3.

Lausanne

1. INTRODUCTION

To study basic phenomena in plasma physics, large volumes of collisionless, quiescent and uniform plasmas are needed. The plasma is normally produced by an r.f. discharge (Hirshfield et al., 1971) or by collisional ionization with electrons from heated filaments (Taylor et al., 1972). r.f. plasmas are quite noisy, whereas the filament-created plasmas are quiescent but require enormous heating powers to maintain densities of the order of 10^9 cm^{-3} without confinement. However, the use of "magnetic walls" as described by Limpaecher and MacKenzie (1971, 1973) drastically reduces this power without introducing additional noise into the plasma. In this report we describe a plasma box based on the magnetic multipole confinement principle.

2. APPARATUS

The device consists of a 183 lt vacuum chamber, in which a rectangular box of 36 x 36 x 60 cm^3 covered with 434 permanent magnets is inserted (figure 1). There exist two types of magnets, metallic and ceramic ones. Metallic magnets show a high remanent induction, whereas the ceramic material is specified by a high coercive force (figure 2). In order to find the appropriate material, the load line has to be found, i.e. the operating point on the demagnetization curve. Solving Maxwell's equations

$$\oint \vec{H} \cdot d\vec{\ell} = 0 \quad , \quad \oint \vec{B} \cdot d\vec{F} = 0 \tag{1}$$

for an open magnetic circuit, the slope of the load line becomes

$$tg\,\alpha = \frac{F_o}{F_i}\,\frac{\ell_i}{\ell_o} \quad . \tag{2}$$

The indices i and o design values inside and outside the magnet, respectively. Stray factors, taking into account that not all flux lines come out at the pole faces, are neglected.

Equation (2) depends only on geometric factors of the magnet. Considering $\frac{F_o}{F_i \ell_o}$ as approximately constant, α decreases with decreasing magnet length l_i. If short magnets are to be used, the operating point on the B-H curve lies always on the left of the intersection point of the two demagnetization curves; therefore the attainable induction is higher with ceramic magnets.

Our multipole field is provided by cheap Ferroxdure disk magnets with a diameter of 45 mm and a length of 9 mm. To avoid strong outgasing of the porous ceramic material, each magnet is in its own small pillbox. The magnets are arranged with alternating polarity in a closest-packed layer, creating a confining field which drops off exponentially towards the interior of the volume. The rectangular magnet supporting box is made of mild steel on which the magnets are held by their own magnetic attraction. By using mild steel, the field lines are short-circuited on one side of the magnets and the field is increased at the pole face from 500 Gauss to 900 Gauss.

The plasma is produced by electron emission from negatively biased filaments. The magnet pole faces serve as anodes. The surface of the filament supports is insulated with glass tubes. To determine the emission current, i.e., the total filament surface necessary to obtain a certain ion density, a rate equation is employed where in a steady state the ion production rate must equal the loss rate.

The production rate is given by

$$\frac{dn_{ip}}{dt} = \frac{n_o \sigma \lambda I_e}{eV} \qquad (3)$$

n_o is the neutral density, σ the ionization cross section, λ the effective primary electron mean free path and V the volume of the box. The loss rate is

$$\frac{dn_{ie}}{dt} = \frac{n_i v_i F}{V} \quad , \qquad (4)$$

where v_i is the ion thermal velocity and F is the open surface of the cusps through which the plasma is leaking out. Neglecting all electric effects Berkowitz et al. (1958) and Grossmann (1966) found an open diameter of a cusp of the order of the ion cyclotron radius and the total open surface for N cusps becomes

$$F = N\pi \left(\frac{m_i v_i}{eB}\right)^2 \tag{5}$$

From (3) and (4) the rate equation is

$$\frac{dn_i}{dt} = -\frac{n_i v_i F}{V} + \frac{n_o \sigma \lambda I_e}{eV} \tag{6}$$

which admits as a steady state solution

$$n_i = \frac{n_o \sigma \lambda \tau I_e}{eV} \tag{7}$$

τ is the time constant, defined by

$$\tau = \frac{V}{v_i F} = \frac{V(eB)^2}{\sqrt{27}\pi N m_i^{1/2} (kT_i)^{3/2}} \tag{8}$$

Inserting typical values into equation (8), V = 78 x 10^3 cm^3, B = 900 Gauss, N $\simeq$ 500, m_i = 40 x m_p, kT_i = 0.5 eV, the time constant comes out to be of the order of 200 μs. To obtain an ion density n_i = 10^9 cm^{-3} at a neutral pressure of 10^{-4} Torr, an emission current of $I_e \sim 200$ mA is necessary. The ionization cross section used is given in figure 3 and λ is supposed to be of the order of three to four times the box dimension (Limpaecher and MacKenzie, 1973).

Such an emission current is easily produced by four tungstene filaments with a total length of 16 cm and a diameter of 0.4 mm.

3. RESULTS

The electron temperature and density were measured with a flat movable Langmuir probe of area 0.197 cm^2. The characteristic was displayed on an oscilloscope or plotted with an x, y recorder using a probe driver described by Auvray (1972). The oscilloscope display of a typical Langmuir trace is given in figure 4.

An electrostatic analyzer is employed in order to measure the ion temperature and density (Ikezi and Taylor, 1970). It consists of three fine mesh grids (78 lines/cm, 34 % transparency) and a collector. The separation between the first two grids is 0.5 mm, between the second and third grid and the collector 1 mm. The first grid is at floating potential (a.c. grounded), the energy selection sweep is applied to the second grid, while the negative third grid acts as an electron suppressor for plasma electrons as well as for secondary electrons emitted from the collector. An oscilloscope display is shown in figure 5.

Two series of measurements were made: one with grids of 60 % transparency at zero potential around the negatively biased filaments in order to prevent a direct contact of the plasma with the cathode and an other without any shielding. Electron densities for typical operating pressures, fixed electron emission current and acceleration voltage are shown in figure 6. The shielding reduces the plasma density roughly by a factor of two. In figure 7 a plot of the electron temperature and the plasma potential versus neutral pressure is given. The shielding grids collect electrons of the tail of the distribution function and the temperature is lowered. The plasma potential with shielded filaments is always positive and approximately constant.

The variation of V_p can be interpreted using cusp containment theory. Electrons escape more rapidly through the cusps than the ions, due to their higher velocity. To conserve charge neutrality, an ambipolar electric field parallel to the magnetic field will be established. The plasma potential becomes positive and the ion loss is slightly increased, whereas the electron loss is reduced

by $\exp\left\{-eV_p/kT_e\right\}$. The shielding grids increase the open surface and the plasma potential has to be more positive to conserve charge neutrality. The negative potential for the low density conditions without shielding may be caused by the negatively biased filaments. Increasing the plasma density increases the electron and ion fluxes and decreases the temperature. In order to keep the factor $I_e \exp\left\{-eV_p/kT_e\right\}$ roughly constant, the plasma potential must become more positive as may be seen from figure 7.

The behaviour of the electron density, the electron temperature and the plasma potential as a function of the filament emission current are plotted in figures 8 and 9. For the unshielded filaments the electron temperature and the plasma potential show a saturation, while the density is still increasing. In figures 10 and 11 we give plasma density, electron temperature and plasma potential as a function of the primary electron acceleration voltage with constant neutral pressure and emission current. From figure 10 a maximum of the ionization cross section at 90 V is apparent, while from figure 11 the electron energy remains approximately constant.

In all measurements the ion temperatures given by the electrostatic analyzer are quite high, between 0.6 eV and 0.9 eV, a result which was confirmed by launching ion acoustic waves.

The following table summarizes some characteristic values under typical operating conditions:

	Shielded filaments	Unshielded filaments
Residual gas pressure	5×10^{-7} Torr	5×10^{-7} Torr
Argon pressure	2×10^{-4} Torr	2×10^{-4} Torr
Electron acceleration voltage	- 100 V	- 100 V
Emission current	160 mA	160 mA
Filament heating power	200 VA	200 VA
Plasma density	4.5×10^{8} cm^{-3}	2.1×10^{9} cm^{-3}
Electron temperature	1.5 eV	2.3 eV
Ion temperature	-	0.7 - 0.8 eV
Plasma potential	+ 2V	+ 0.5 V

Table: Characteristic plasma parameters for typical operating conditions.

The homogeneity of the plasma was checked with the movable Langmuir probe and seems to be better than 1 % over a distance of 25 cm. The noise level $\langle \delta n/n \rangle$ is of the order of 3×10^{-4} as indicated by a cylindrical Langmuir probe of 0.4 mm diameter.

To determine the plasma lifetime, an acceleration voltage step was created by short-circuiting a series resistor in the path of the emission current (figure 12). The voltage step changes the ionization cross section from σ to $\sigma - \varepsilon(t)\Delta\sigma$, where $\varepsilon(t)$ is the unit step function. The jump of the cross section changes the plasma density which is displayed as a function of time on the oscilloscope. By imposing only a small step, the plasma potential is not changed as it would be the case by turning off the whole acceleration voltage. Applying Laplace

transform to equation (6), the plasma density jump is given by

$$n_i(t) - n_{io} = - \frac{n_o \lambda \Delta\sigma \tau I_e}{eV} \left(1 - e^{-t/\tau}\right) \qquad (9)$$

from which the lifetime may be deduced. A measured Langmuir trace is given in figure 13, the upper curve showing the plasma density decay and the lower curve the applied acceleration voltage step. The time constant found is $\tau \sim 200\ \mu s$.

To confirm this confinement time, we measured the loss rate by electrically insulating one magnet from his neighbours. The collected current, with zero bias at the magnet, was compared with the current drawn by a flat Langmuir probe at zero potential immersed in the field free plasma. The radius of the open surface of a cusp under the operating conditions given in the table above is 2.33 mm and is smaller than the ion cyclotron radius (6 mm for kT_i = 0.7 eV). Defining a mean escape velocity by

$$\bar{v} = \frac{I}{neF} \qquad (10)$$

with the current I collected by the magnet and the cusp surface F, the time constant may be determined from equation (8). $\bar{v}$ contains the effects of the ambipolar electric field. The time constant obtained is $\tau \sim 180\ \mu s$, consistent with the value found above. The plasma leaking out at the point of zero magnetic field between the magnets is smaller than the leakage through a cusp by a factor of 10^3.

Using equation (7), the primary electron mean free path is of the order of $\lambda \sim 3.7$ m, indicating that the primaries are partly confined and collide about 10 times with the walls. By decreasing the neutral pressure to about 2×10^{-5} Torr, the discharge can no longer be maintained and the collected emission current diminishes due to the fact that the plasma potential becomes very negative. The potential drop between filament and plasma is thus decreased and the primary electron energy is not sufficient any longer to ionize the neutral gas.

In order to increase the temperature ratio T_e/T_i a Maxwell demon (MacKenzie et al., 1971) was introduced into the plasma. Our demon consists of a grid (2 lines/cm, wire 0.035 mm) covering an area of 14 x 28 cm^2. Figure 14 shows the efficiency of the demon with and without shielding of the filaments. The efficiency is drastically reduced when the plasma is allowed to be in contact with the cathode. In this case, the demon influences strongly the plasma potential, because his active surface (34 cm^2) is too large compared with the total open surface (75 cm^2) of all the cusps. However, shielding the filaments with grids of a surface of 100 cm^2, the plasma potential increases more slowly (figure 15) and the demon is able to capture the cold electrons. Reducing the demon surface by a factor of two no filament shielding is necessary, the plasma potential now being determined by the cusp surfaces (figure 16). An estimate of the collected current using cylindrical Langmuir probe theory agrees well with the measured current given in figure 15. The demon changes the electron temperature in about 100 μs, consistent with the energy equipartition time between the electrons.

4. CONCLUSIONS

The total open surface in our multipole device is approximately 80 cm^2, while the total box surface is 11200 cm^2. Thus we have an improvement over an unconfined plasma by a factor of 140 and very low electron emission currents are necessary to obtain reasonable plasma densities. The location of the electron emitting filaments is not critical, because the "magnetic walls" do not allow density gradients to be established.

ACKNOWLEDGMENTS

We wish to thank H. Ripper and J.-P. Perotti for the construction of the multipole device and the various electronic parts. We acknowledge also useful discussions with Dr. M. Bitter and Prof. E.S. Weibel.

This work was supported by the Swiss National Science Foundation.

REFERENCES

AUVRAY J. (1972), Laboratoire de Physique des Milieux Ionisés, Ecole Polytechnique Paris, report PMI 574, p. 22

BERKOWITZ J., GRAD H. and RUBIN H. (1958), Proc. Second U.N. Conference on the Peaceful Uses of Atomic Energy, Geneva, 31, 177

GROSSMANN W. (1966), Phys. Fluids 9, 2478

HIRSHFIELD J.L., JACOB J.H. and BALDWIN D.E. (1971), Phys. Fluids 14, 615

IKEZI H. and TAYLOR R.J. (1970), Phys. Fluids 13, 2348

MacKENZIE K.R., TAYLOR J.R., COHN D., AULT E. and IKEZI H. (1971), Appl. Phys. Lett. 18, 529

LIMPAECHER R. and MacKENZIE K.R. (1971), Proc. 3rd Int. Conf. Quiescent Plasmas, Elsinore, Denmark, Sept. 20-24, p. 22

LIMPAECHER R. and MacKENZIE K.R. (1973), Rev. Sci. Instrum. 44, 726

LOTZ W. (1967), Astrophys. J., Suppl. 128, Vol. XIV, 207

TAYLOR R.J., MacKENZIE K.R. and IKEZI H. (1972), Rev. Sci. Instrum. 43, 1675.

FIGURE CAPTIONS

Figure 1: Geometry of the plasma box with dimensions 36 x 36 x 60 cm^3. The disk shaped magnets are arranged in a closest-packed layer. Four filaments are used to maintain densities of $n \sim 10^9$ cm^{-3}.

Figure 2: Demagnetization curves of metallic (Ticonal) and ceramic (Ferroxdure) magnets with load line.

Figure 3: Ionization cross sections for He, Ar and Xe (Lotz, 1967).

Figure 4: Oscilloscope display of a typical Langmuir curve.

Figure 5: Oscilloscope display of a typical ion energy analyzer curve.

Figure 6: Electron densities vs neutral Argon pressure. The residual gas pressure is 5×10^{-7} Torr, the filament emission current I_e = 160 mA and the electron acceleration voltage V_{acc} = 100 V.

Figure 7: Electron temperatures and plasma potential vs neutral Argon pressure for I_e = 160 mA and V_{acc} = 100 V.

Figure 8: Electron densities vs filament emission current for an Argon pressure of 2×10^{-4} Torr and V_{acc} = 100 V.

Figure 9: Electron temperature and plasma potential vs filament emission current for an Argon pressure of 2×10^{-4} Torr and V_{acc} = 100 V.

Figure 10: Electron density vs acceleration voltage for an Argon pressure of 2×10^{-4} Torr and I_e = 160 mA.

Figure 11: Electron temperature and plasma potential vs electron acceleration voltage for an Argon pressure of 2×10^{-4} Torr and $I_e = 160$ mA.

Figure 12: Circuit producing a small potential step on the acceleration voltage.

Figure 13: Upper trace: current on a biased Langmuir probe
Lower trace: acceleration voltage step.

Figure 14: Electron temperature as a function of the demon voltage (demon dimension 14 x 28 cm^2).

Figure 15: Plasma potential and current collected by the demon as a function of applied potential (demon dimension 14 x 28 cm^2).

Figure 16: Electron temperature, plasma potential and collected current as a function of the demon voltage (demon dimension 14 x 14 cm^2).

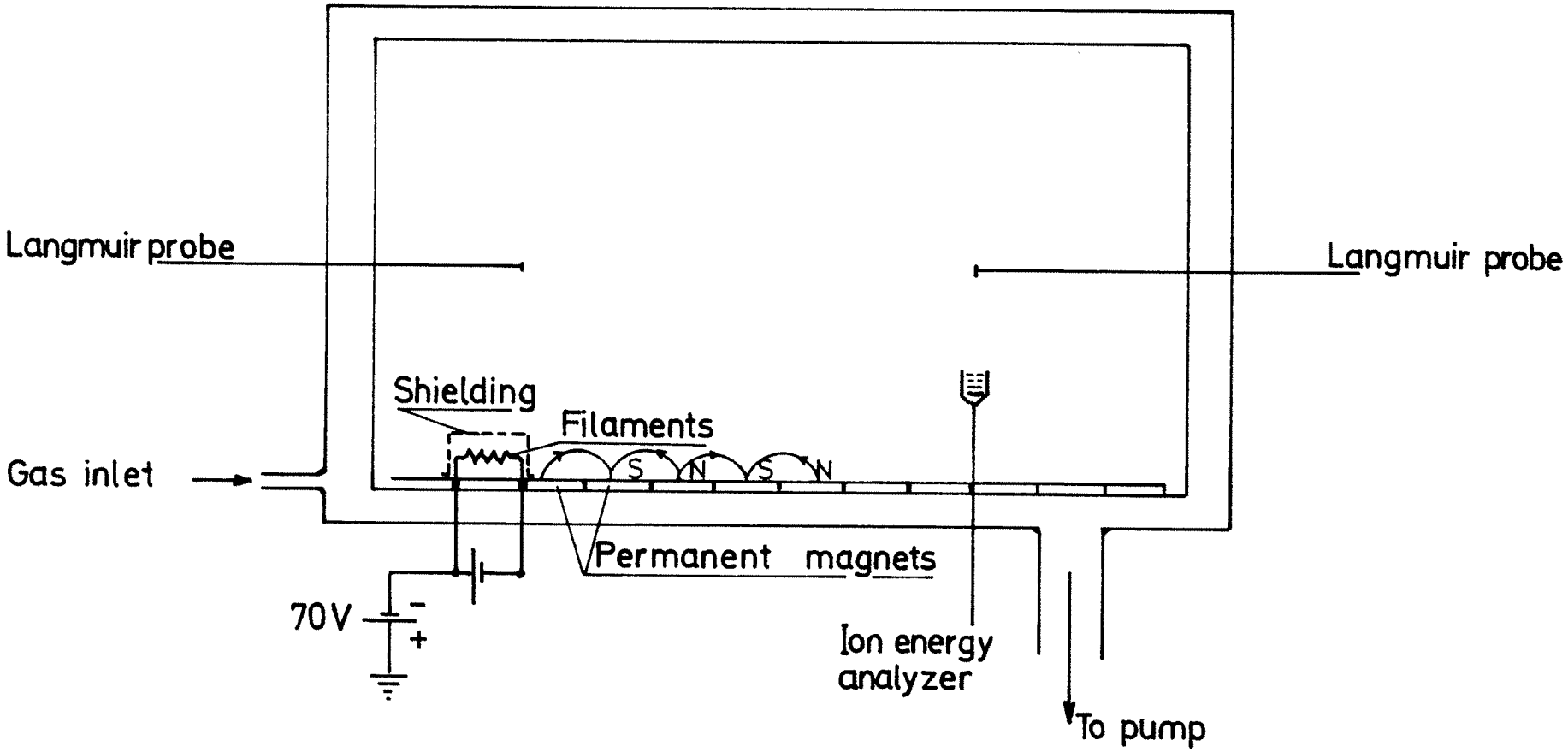
Langmuir probe
Langmuir probe
Shielding
Filaments
Gas inlet
S
N
S
N
Permanent magnets
70V
-
+
Ion energy analyzer
To pump

Figure 1

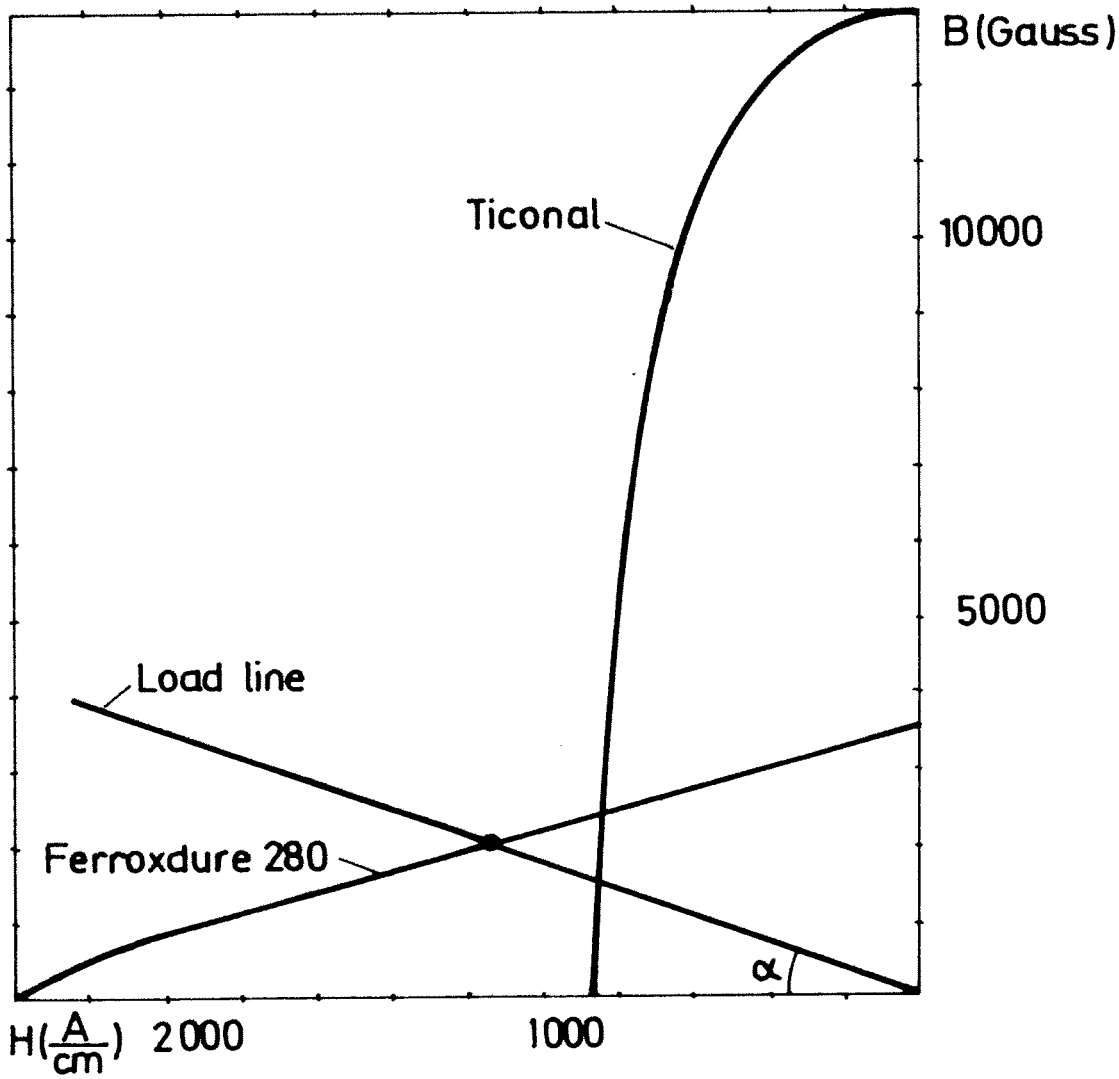
B(Gauss)
Ticonal
10000
5000
Load line
Ferroxdure 280
α
H(A/cm) 2000
1000

Figure 2

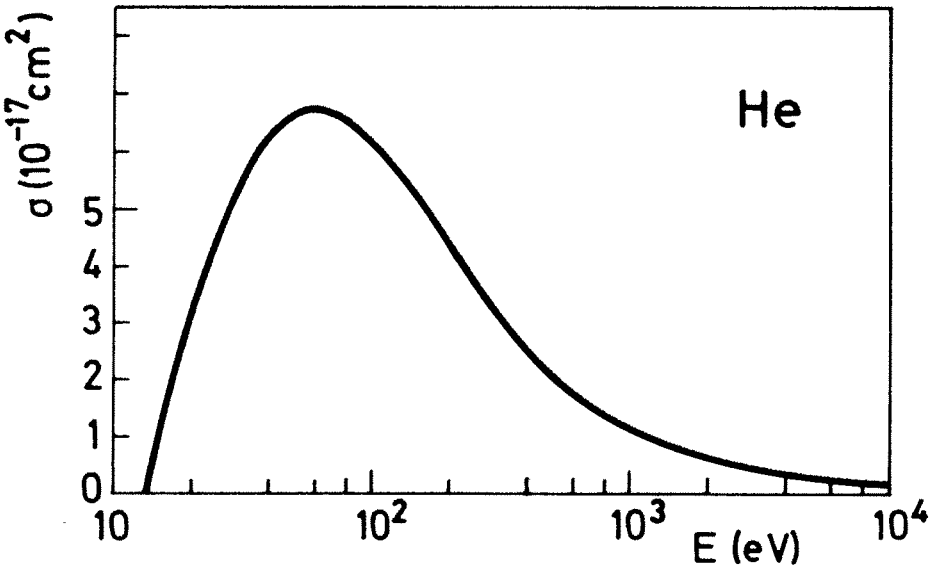
He
σ(10^-17 cm^2)
0
1
2
3
4
5
10
10^2
10^3
10^4
E (eV)

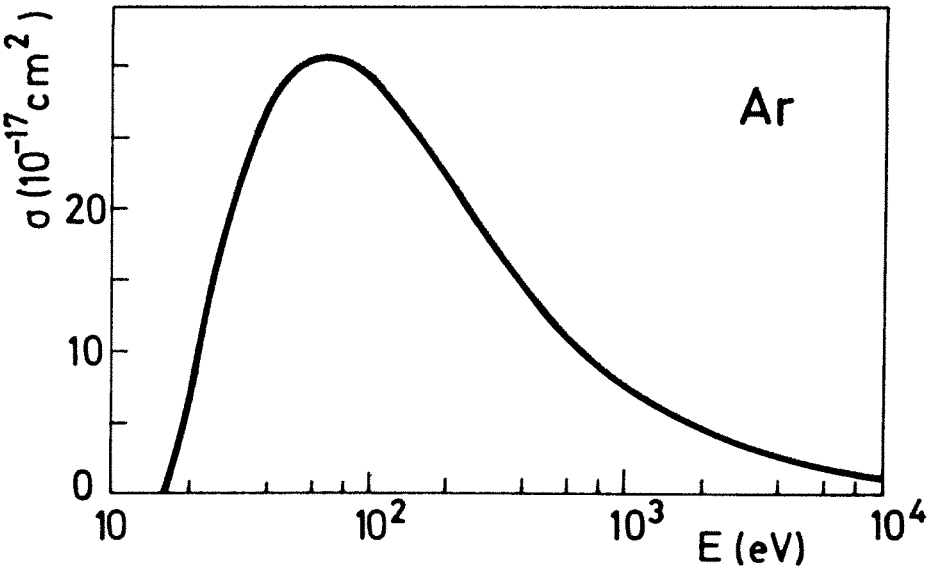
Ar
σ(10^-17 cm^2)
0
10
20
10
10^2
10^3
10^4
E (eV)

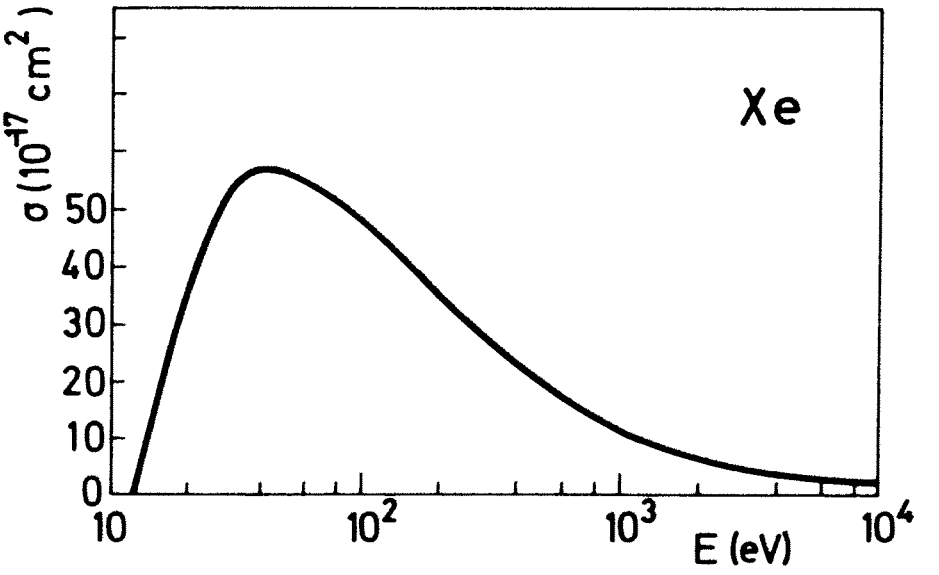
Xe
σ(10^-17 cm^2)
0
10
20
30
40
50
10
10^2
10^3
10^4
E (eV)

Figure 3

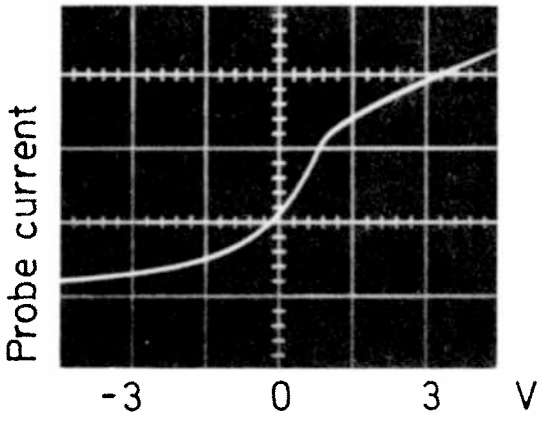

Figure 4

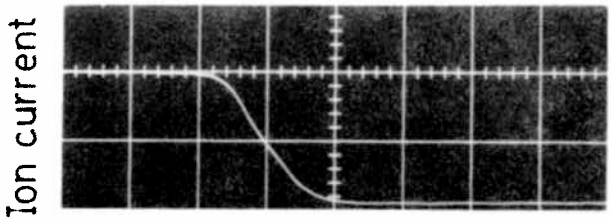

Figure 5

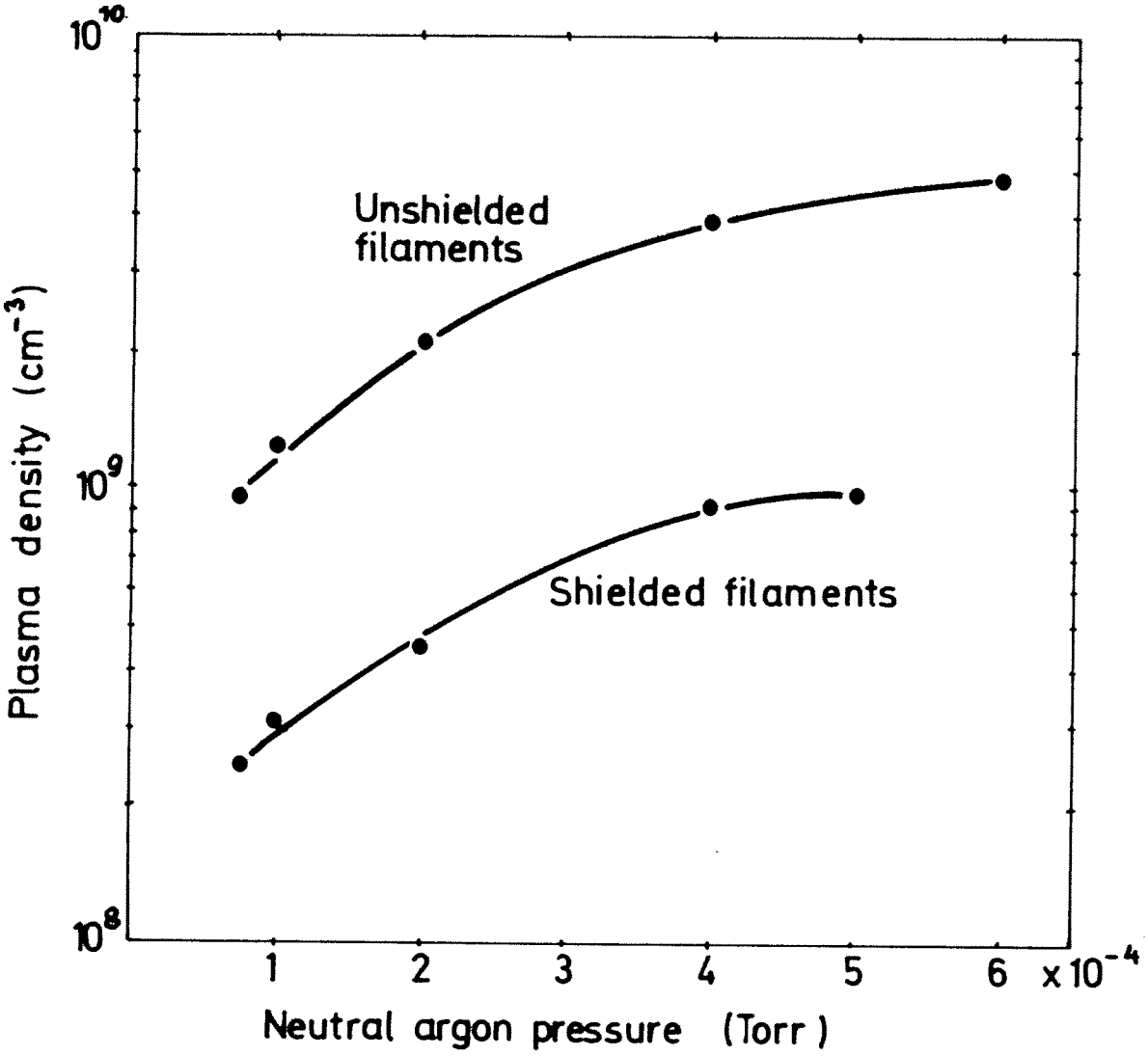
10^{10}
10^{9}
10^{8}
Plasma density (cm^{-3})
Unshielded filaments
Shielded filaments
1
2
3
4
5
6
x 10^{-4}
Neutral argon pressure (Torr)

Figure 6

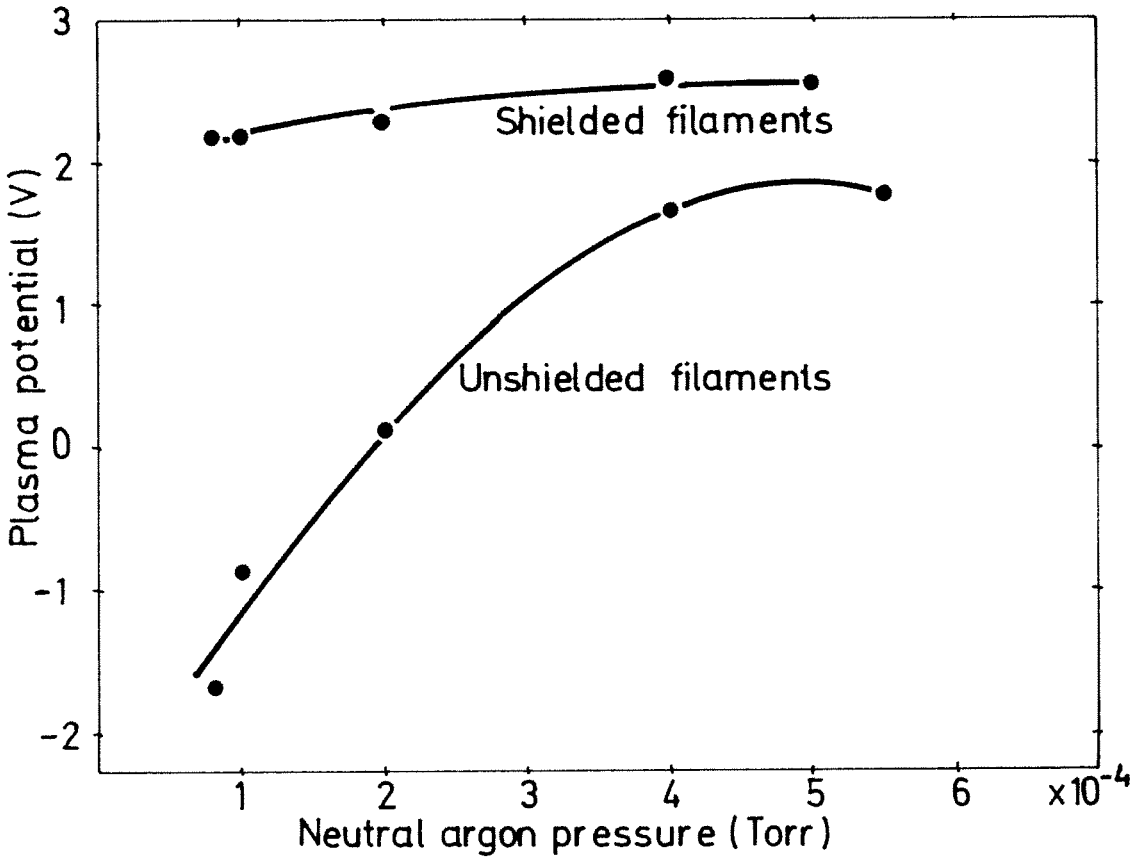
Shielded filaments
Unshielded filaments
Plasma potential (V)
3
2
1
0
-1
-2
1
2
3
4
5
6
x10⁻⁴
Neutral argon pressure (Torr)

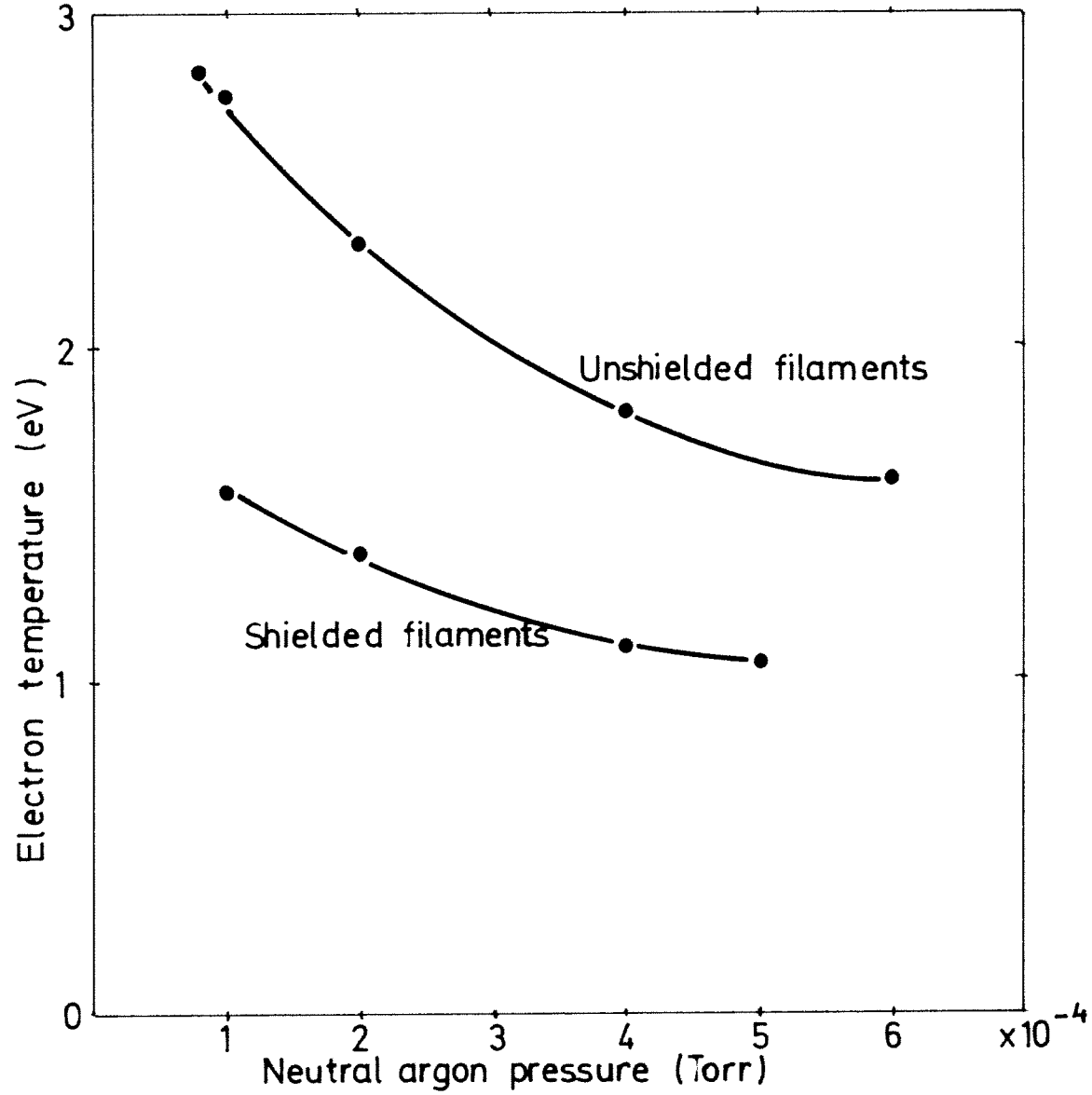
Unshielded filaments
Shielded filaments
Electron temperature (eV)
3
2
1
0
1
2
3
4
5
6
x10⁻⁴
Neutral argon pressure (Torr)

Figure 7

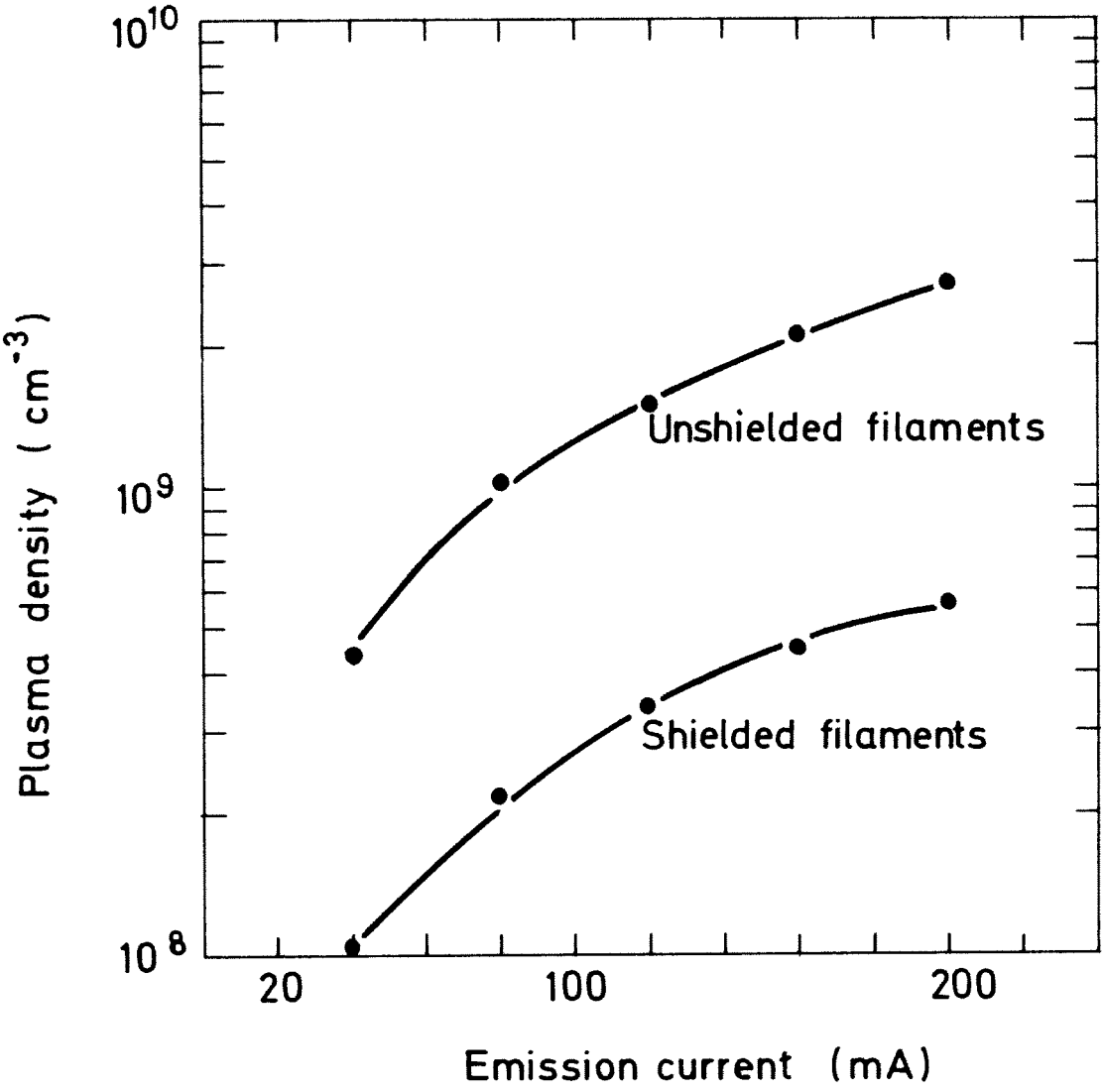
10^{10}
10^{9}
10^{8}
Plasma density (cm^{-3})
Unshielded filaments
Shielded filaments
20
100
200
Emission current (mA)

Figure 8

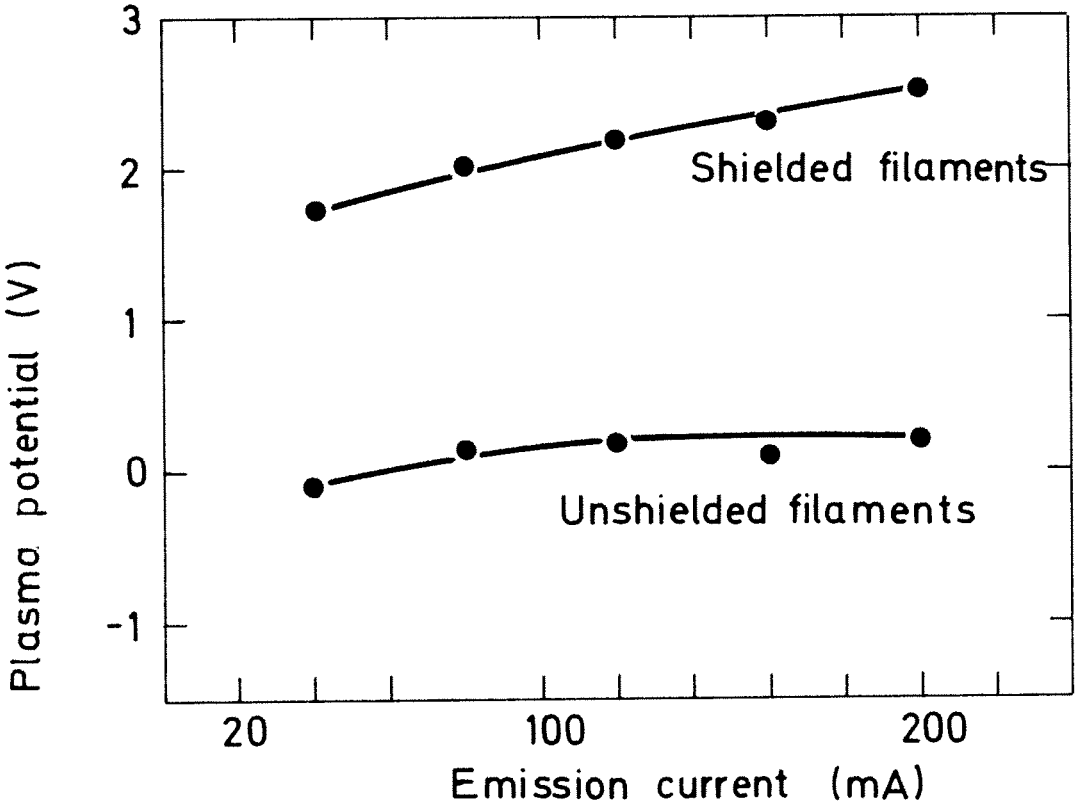
3
2
1
0
-1
Plasma potential (V)
Shielded filaments
Unshielded filaments
20
100
200
Emission current (mA)

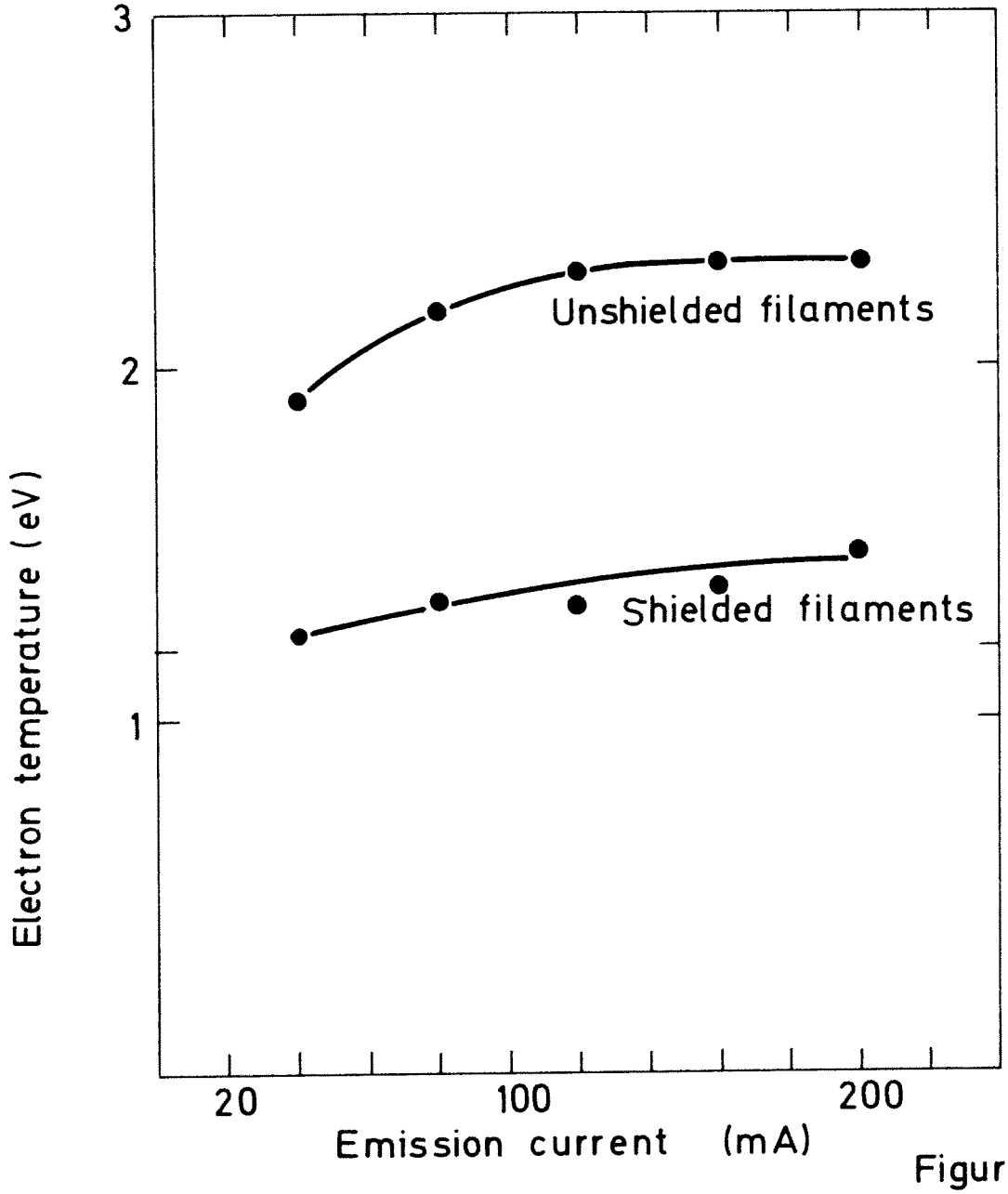
3
2
1
Electron temperature (eV)
Unshielded filaments
Shielded filaments
20
100
200
Emission current (mA)

Figure 9

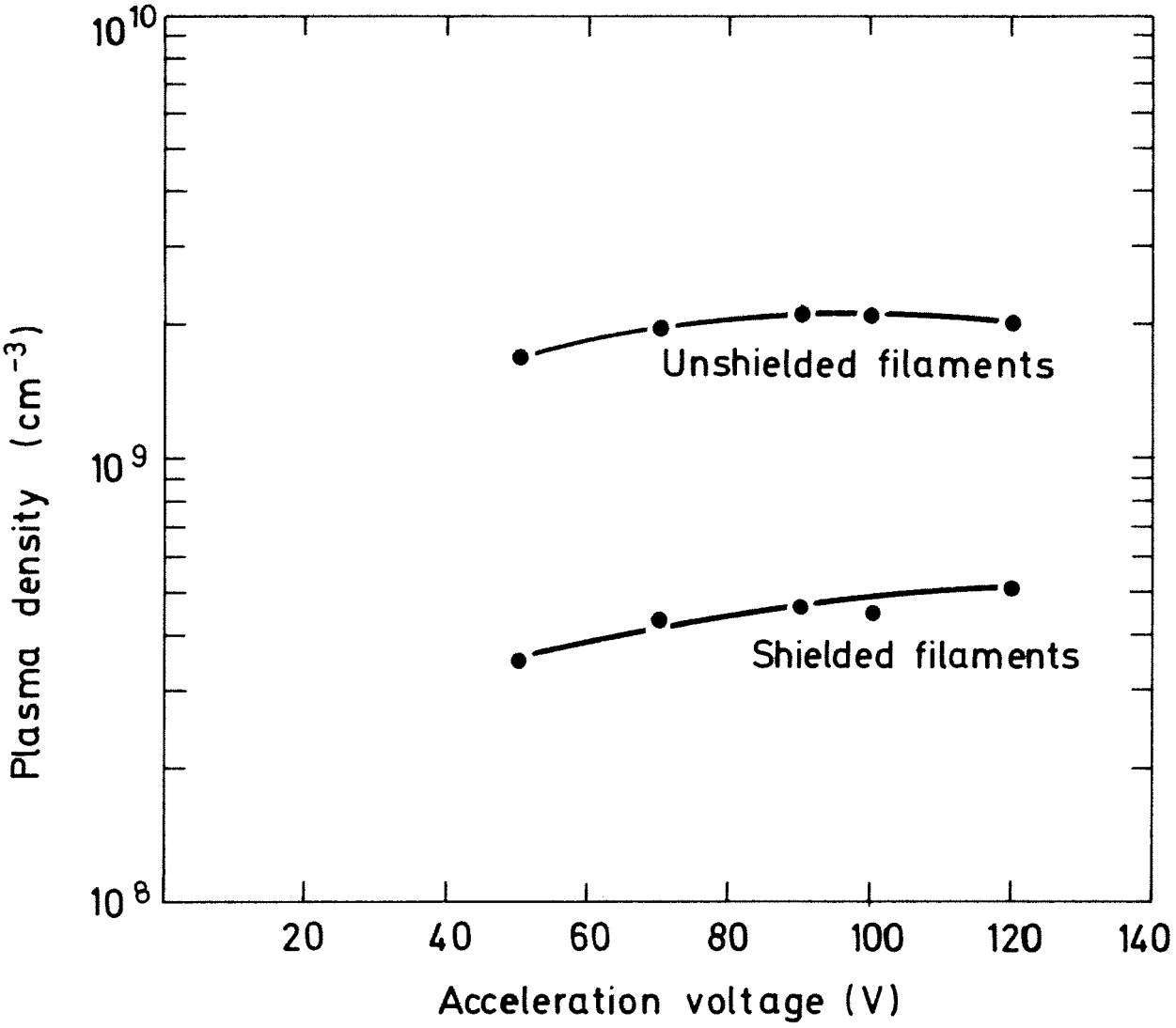
10^{10}
10^{9}
10^{8}
Plasma density (cm^{-3})
Unshielded filaments
Shielded filaments
20
40
60
80
100
120
140
Acceleration voltage (V)

Figure 10

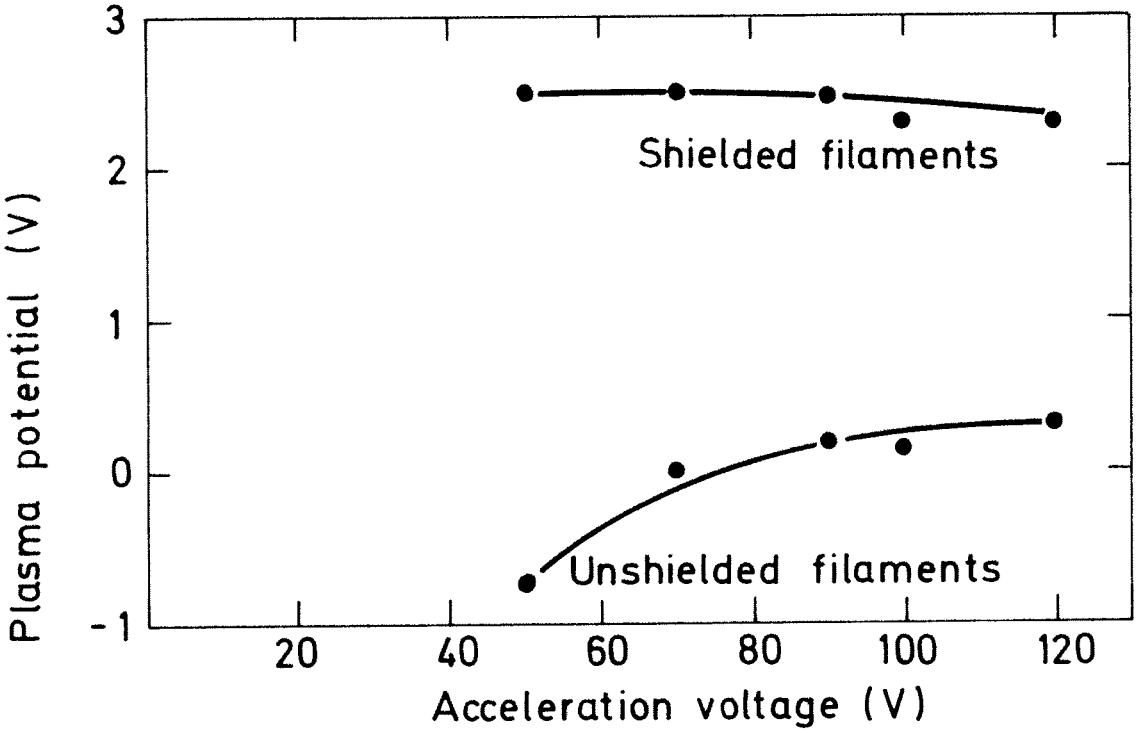
Plasma potential (V)
3
2
1
0
-1
Shielded filaments
Unshielded filaments
20
40
60
80
100
120
Acceleration voltage (V)

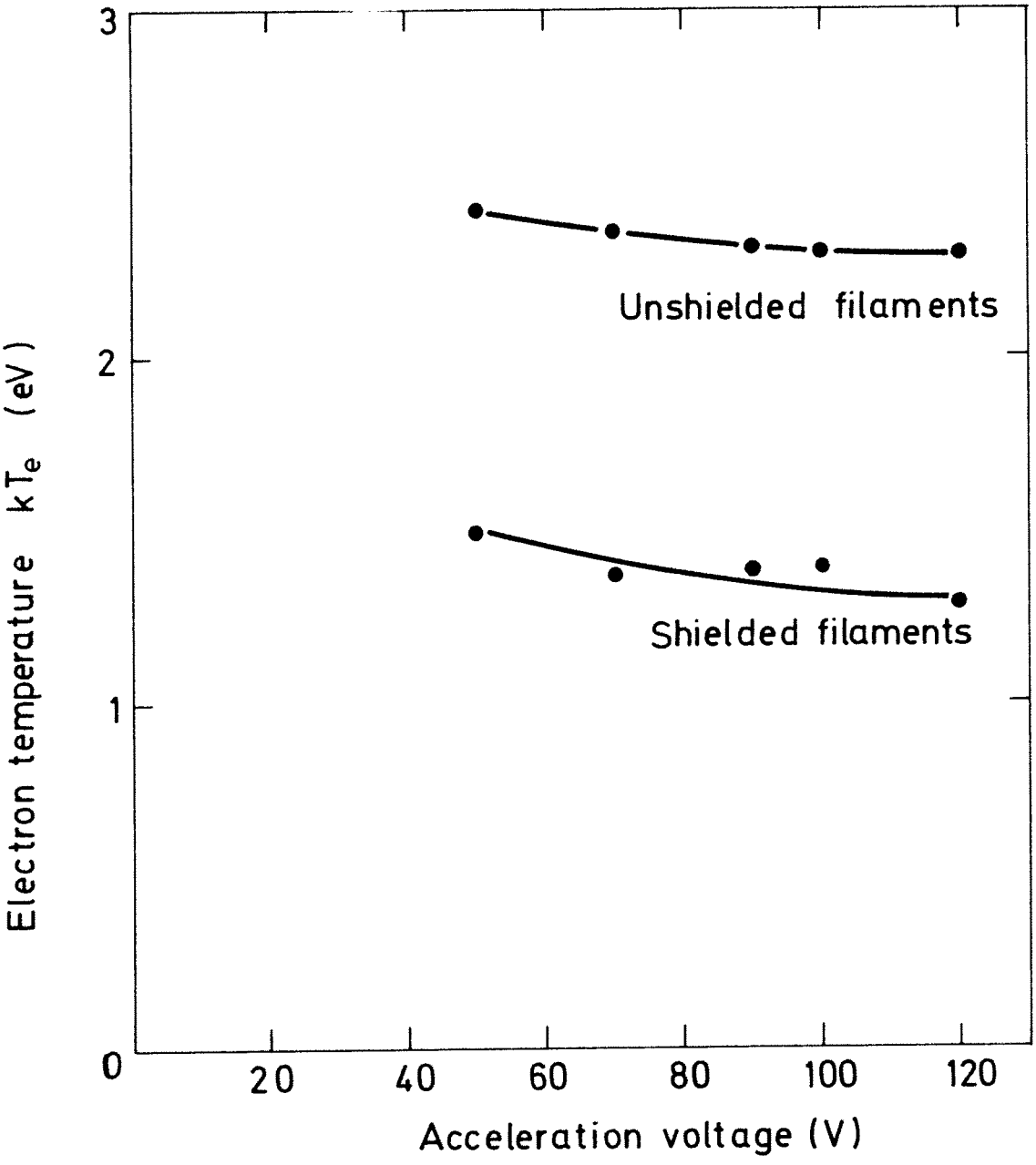
Electron temperature kTe (eV)
3
2
1
0
Unshielded filaments
Shielded filaments
20
40
60
80
100
120
Acceleration voltage (V)

Figure 11

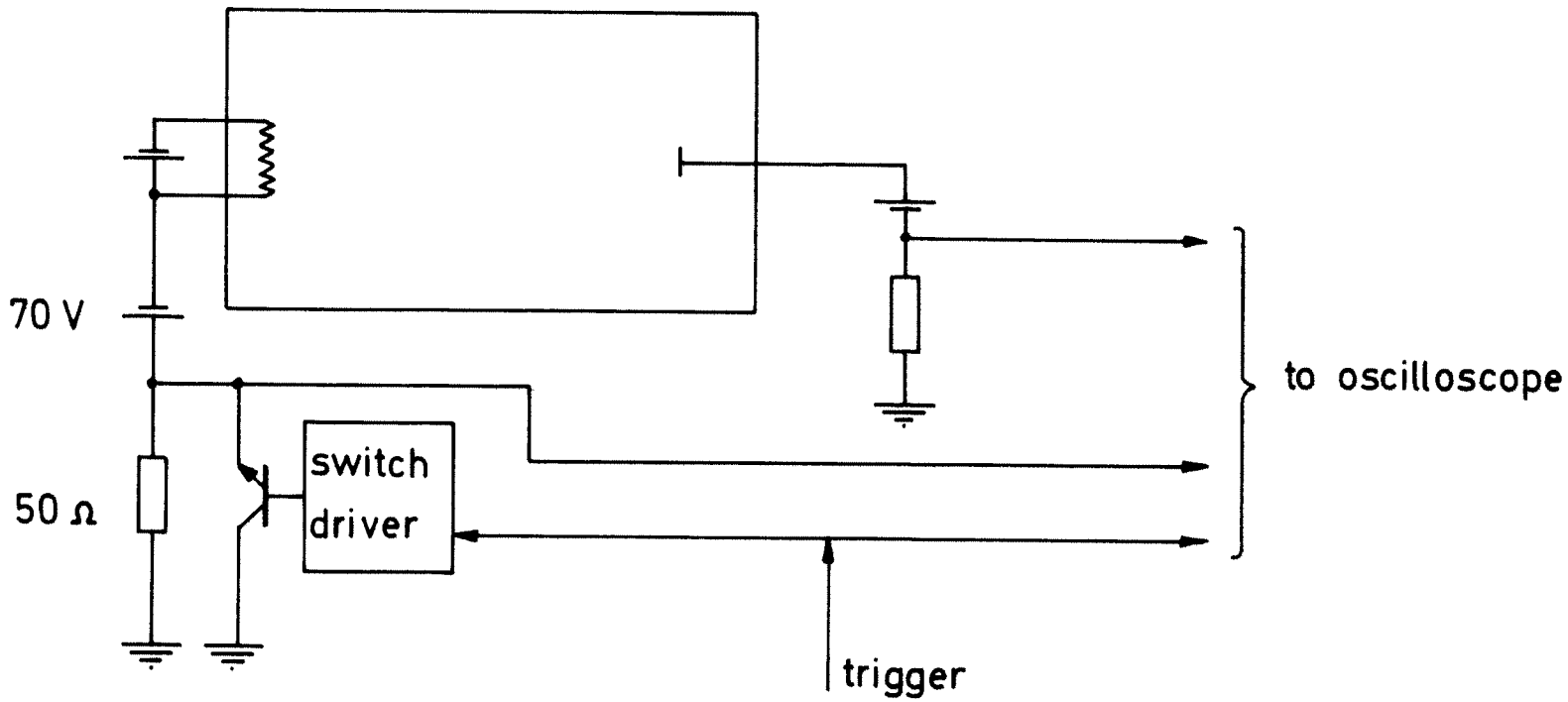

Figure 12

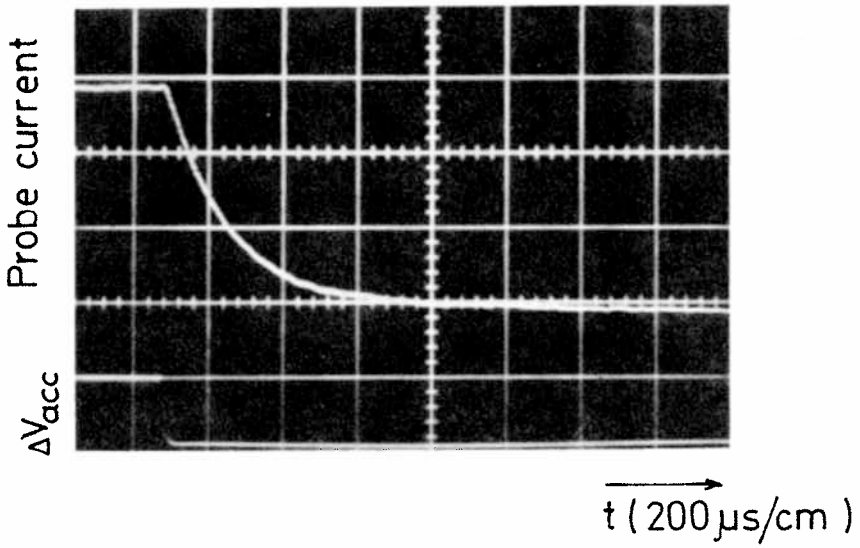

Figure 13

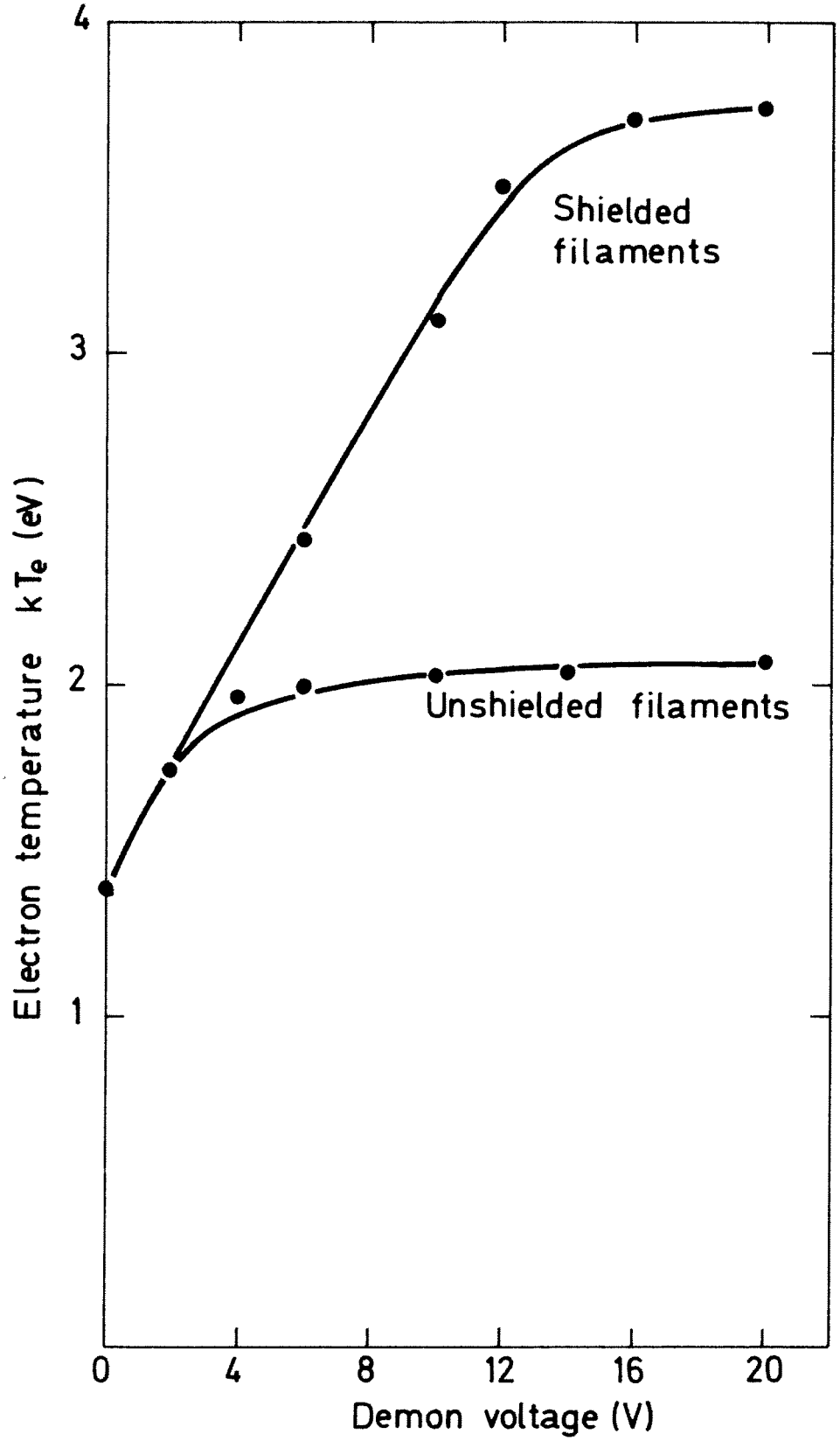
4
3
2
1
Electron temperature kT_e (eV)
Shielded
filaments
Unshielded filaments
0
4
8
12
16
20
Demon voltage (V)

Figure 14

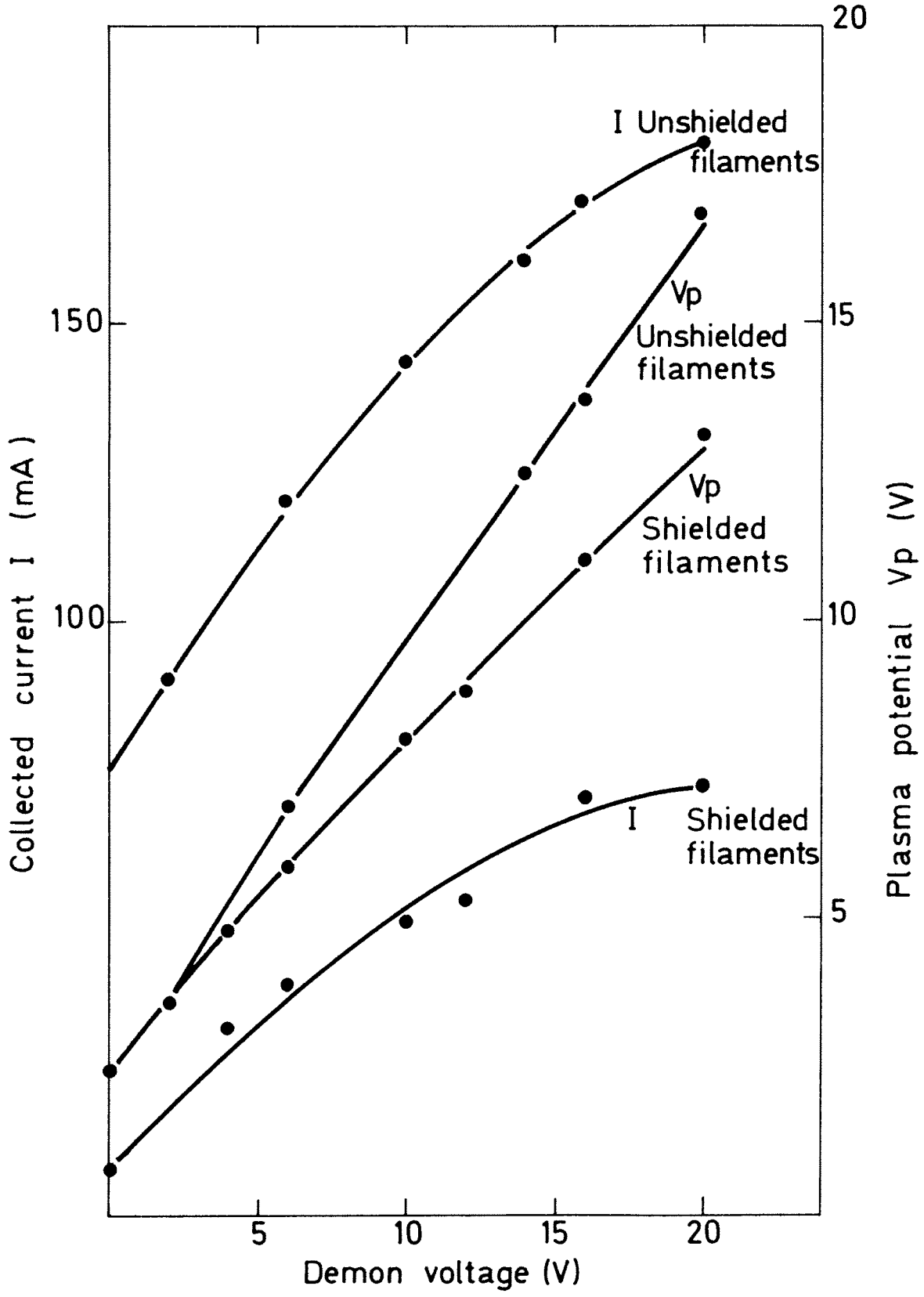
I Unshielded filaments
Vp Unshielded filaments
Vp Shielded filaments
I Shielded filaments
Collected current I (mA)
Plasma potential Vp (V)
Demon voltage (V)
150
100
20
15
10
5
5
10
15
20

Figure 15

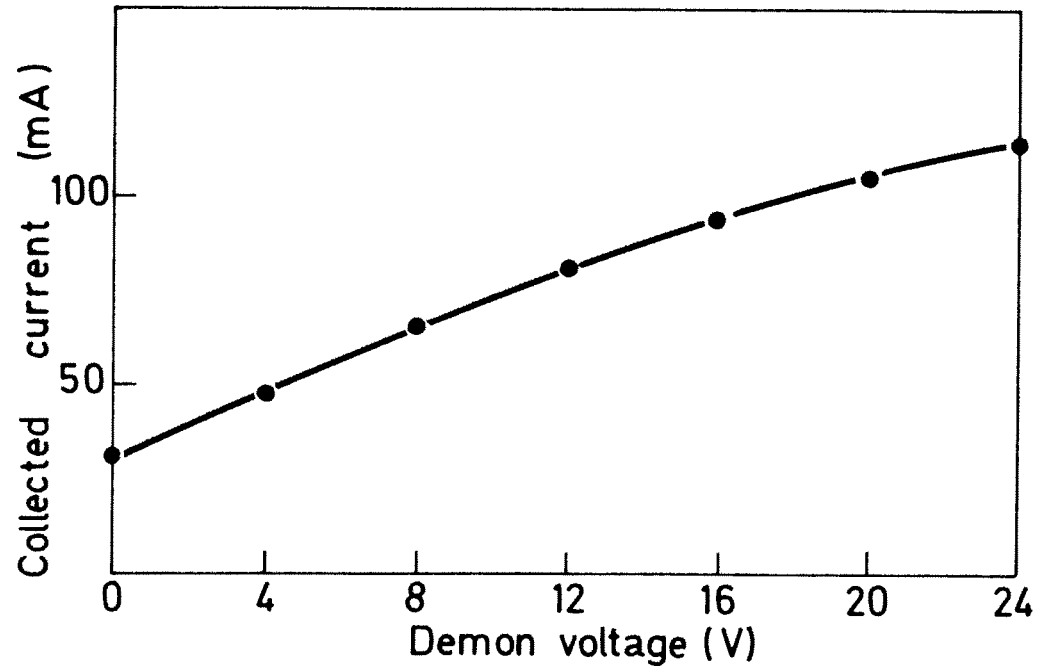
Collected current (mA)
100
50
0
4
8
12
16
20
24
Demon voltage (V)

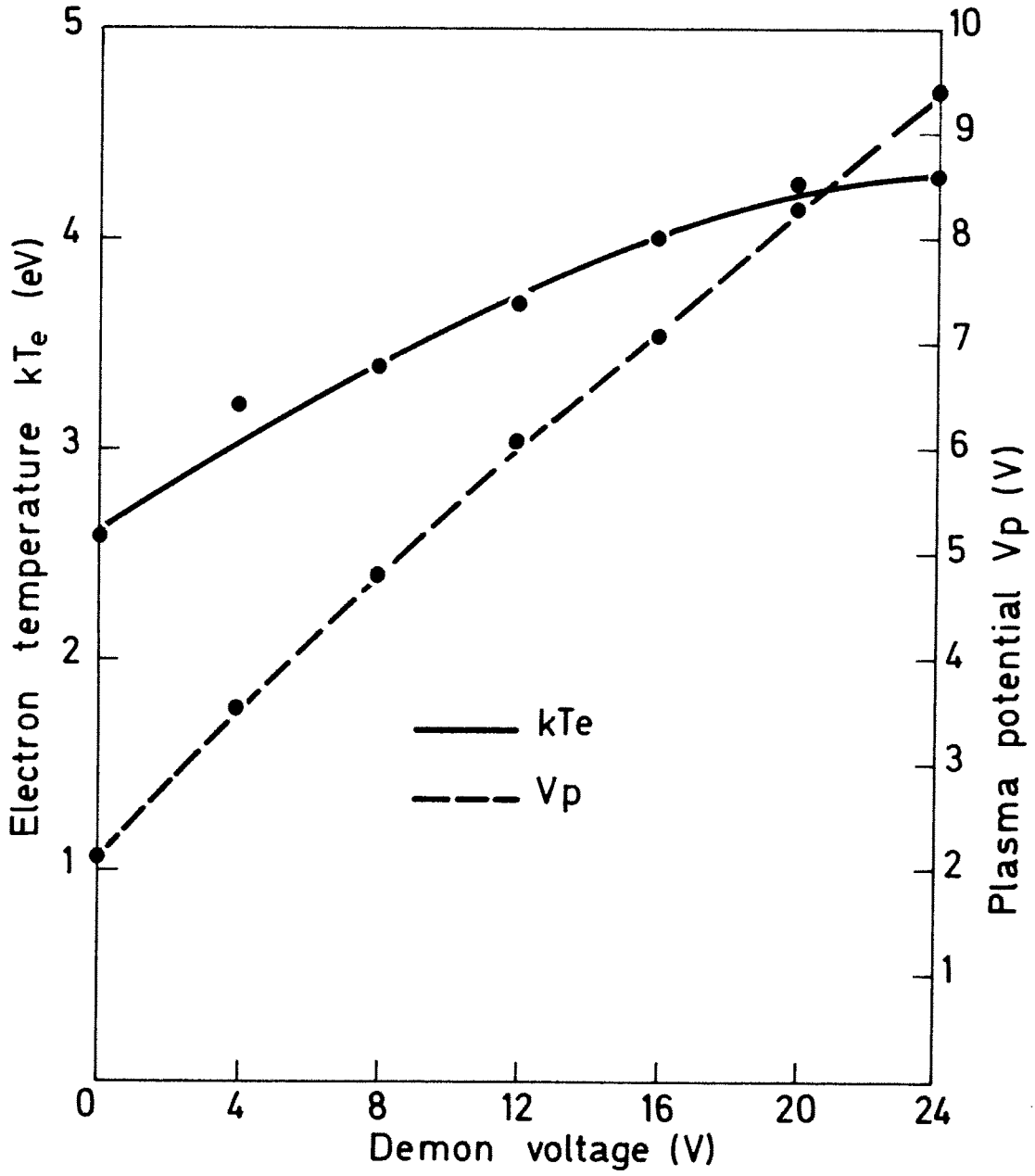
Electron temperature kTe (eV)
Plasma potential Vp (V)
5
4
3
2
1
10
9
8
7
6
5
4
3
2
1
kTe
Vp
0
4
8
12
16
20
24
Demon voltage (V)

Figure 16